E10-96-288

A.Astvatsaturov, J.Budagov, V.Shigaev, M.Bosman[1],
M.Nessi[2], D.Pantea[3]

IDENTIFICATION OF b-JETS WITH A LOW p_T MUON USING ATLAS TILE CALORIMETER SIMULATION DATA AND ARTIFICIAL NEURAL NETWORKS TECHNIQUE

[1]IFAE, Barcelona, Spain
[2]CERN, Geneva, CH-1211, Switzerland
[3]IAP, P.O.Box MG-6, Bucharest, Romania

$Sw_{y}6\mathcal{L}g$

1996

1 Introduction

It was shown in [1], [2] that overall efficiency of b-jets tagging can be substantially increased if soft muons with p_T down to 2-3 GeV/c are efficiently identified inside jets. Such muons cannot be reliably registered by ATLAS muon detector because of significant probability to be absorbed in the calorimeter.

A way to encrease b-tagging efficiency consists in using response data of ATLAS hadron calorimeter (HC) for identification of soft muons. Due to high penetration ability of muons the signal in the last depth (section or longitudinal sample) of the hadron calorimeter should be greater for jets with muons compared with jets without muons (gluon jets, light quark jets).

The task of separation between gluon jets and b-jets (a single soft muon inside a b-jet) was considered in [2] for jets with p_T = 20 and 40 GeV/c in the central region $0 < \eta < 0.6$. It was shown that by imposing a cut on the deposited energy in the last HC section one can reach the rejection factor for gluon jets R_g = 9 (at p_T = 20 GeV/c) and R_g = 4 (at pT=40 GeV/c) with 95% efficiency of b-jets identification. Anticipation was also expressed that at a loss of 10% of b-jets the rejection factor for gluon jets could be pushed up into the region of 50 - 100 if information from the middle section of HC is used in the form of summed energy value of 2 adjacent cells with maximum deposit from a 3 × 3 cell window centered on the position (η_m, ϕ_m) of the cell with the highest deposited energy in the last HC section.

Our aim was to investigate in a systematic way the posibility to enhance the capability of ATLAS Tile Calorimeter to identify low p_T muons inside b-jets by the use of artificial neural networks (ANN) technique.

2 Investigation scheme

In what follows the b-jet events (calorimeter response to b-jets) will be refered to as signal events, and the gluon jet events – as background events respectively.

We have included a rather wide set of jet classifiers (discriminators) into our research program. The classifiers were naturally divided into groups, the study of each group constituted a separate step in our investigation scheme. The steps imply investigation of the next groups of discriminators:

A. Linear threshold discriminator (LTD) operating on summed energy deposition E_4 in the last (4-th) section of HC.

B. Neural net discriminators (NND) operating on longitudinal profile of jet energy deposition in HC.

C. A series of neural net discriminators that make use of information on the distribution of cell energies inside 3 × 3 cell windows in the first and the

middle HC sections (all windows centered on the position (η_m, ϕ_m) of the cell with the highest deposited energy in the last HC section).

D. A series of neural net discriminators that are extensions of discriminators from Group C. These discriminators make use of additional features related to: 1) joint distribution of the 3 × 3 cell window position and the jet axis in (η, ϕ) plane, 2) jet radius as estimated using HC response.

E. Neural net discriminators that operate on full spectrum of feature types used by discriminators from Groups A,B,C,D.

Assignment of a discriminator to a certain group does not depend on the discriminator architecture or its complexity and is guided solely by the type of event features used as inputs to the discriminator. For example, discriminators within Group C differ in the number of their inputs (see below).

In fact each discriminator in Groups C,D,E is a combined discriminator that performs jet classification in two consecuitive stages:

Stage 1. An event is classified in LTD mode with the minimum cut threshold (MCT) applied to the summed energy deposition E_4 in the last HC section (MCT value is defined by noise level). If E_4 of an event is below MCT then the final decision is made at Stage 1: the event is classified as background event (i.e. gluon jet). Otherwise the final decision is made at Stage 2.

Stage 2. An event is classified in NND mode by applying a cut to the neural net output signal.

It follows from this two stage classification scheme that the upper bound ε_b^{max} of b-jet identification efficiency attainable without losing gluon/b-jet separation ability is imposed by characteristics of LTD discriminator. In our case $\varepsilon_b^{max} = 0.94$ for jets at $p_T = 20$ GeV/c and $\varepsilon_b^{max} = 0.96$ at $p_T = 40$ GeV/c. The importance of minimizing additional loss of efficiency ε_b at Stage 2 becomes evident.

At Stage 2 only subsets of jet events that satisfy the condition $E_4 > MCT$ are used for training and testing neural nets. In estimating discriminator characteristics we followed the procedures descibed in details in [3], [4]. The obtained characteristics are later renormalized in regard to the whole sets of events to finally represent characteristics of the combined two stage discriminator.

In the present paper all results obtained with the use of neural nets are given in renormalized form.

3 Simulation data

The same data files were used in the present investigation and in [2]. We remind here some simulation conditions.

1. Single jets were generated in DICE with p_T = 20 and 40 GeV/c uniformly in η in the central region $0 < \eta < 0.6$.

2. Gluon jets were chosen as background process.

3. For b-jets (signal events) some conditions were imposed at particle level at the moment of generation:
a) only events containing one muon (accompanied by its own neutrino) were accepted;
b) transverse momentum of the muon must be in the soft region $2 < p_T < 5$ GeV/c.

4. For simulation, the Technical Proposal layout was used were Tile Barrel Calorimeter consisted of 4 longitudinal depths (sections) - along r axis in cylindrical coordinate system.

5. At each p_T value 500 b-jets and 500 gluon jets were generated.

Because of decision [5] to bring together two central depths of HC, the simulated cell energy depositions in these two HC depths were properly merged.

Distributions of summed energies deposited in each section of ATLAS calorimeter are shown in Fig.1, Fig.2. In comparison with the case of isolated muons and pions [3],[4] the present distributions for the two types of events are much more overlapped in each HC section.

4 Discriminators and their performance

Three-layered perceptrons with n input neurons (nodes) in the first layer, n_h neurons in a hidden layer and one output neuron in the third layer were selected for constructing neural net discriminators. Adjacent layers of the perceptrons are fully interconnected. A formula (n, n_h, 1) will be used to depict the structure of such perceptrons. Actually throughout the present investigation two structures were used: (n, 4, 1) for jets at p_T = 20 GeV/c and (n, 6, 1) at p_T = 40 GeV/c. The package JETNET [8] was used for training the perceptrons.

Inputs to the first layer of NND may be thought as components of n-dimensional vector that represents an event in n-dimensional feature space. Dimension n and ordering of input components are fixed for a particular NND. For neurons in the hidden and output layers the nonlinear neuron activation function $g(a) = (1 + \exp(-2a))^{-1}$ was chosen; hence the perceptrons perform nonlinear mappings of n-dimensional space into (0, 1) interval. During training phase the target value of the output neuron was put to 1 for b-jets and 0 for gluon jets. Training procedure iteratively adjusts weigths of connections

between neurons in order to minimize mean fit error MFE, i.e. mean squared deviation of actual net output values $O_{NN}(p)$ from the target values t(p) over the whole training set of events:

$$MFE = \frac{1}{2N_p} \sum_{p=1}^{N_p} (t(p) - O_{NN}(p))^2$$

where p denotes events.

One pass over training sample constitutes a step of the training procedure; the step is usually called an "epoch". Using a trained perceptron one gets one-dimensional distributions of net output values for b-jets and gluon jets. By applying variable thresholds to neural net output values one gets estimates of important characteristics of discriminators such as:

- ε_b – efficiency of signal events recognition, i.e. the probability that a b-jet event be correctly classified,

- α_b – inefficiency of signal events recognition, i.e. the probability that a b-jet event be misclassified $(\alpha_b = 1 - \varepsilon_b)$,

- β_g – survival probability for background events, i.e the probability that a gluon jet event be misclassified,

- $R_g = 1/\beta_g$ – rejection factor for gluon jets.

Components of input vector for a neural net are usually called event features. Features are functions of raw data items (data items are cell energies of HC response in our case). Evaluation of feature values is an operation called preprocessing of measurement data (or source data).

In the present investigation the performance of various discriminators is considered here in the order defined by our investigation scheme. Since the total number of discriminators is great, we restrict ourselves to presenting only one characteristics for each discriminator, namely the dependence of R_g on ε_b. This functional dependence will be given in the form of plots (R_g, ε_b) prepared with the use of simulated jets.

Group A. This group includes the single discriminator LTD that performs classification by thresholding the summed energy deposition E_4 in the last HC section.

Distributions of E_4 are presented in Fig.3 for both types of simulated jets at $p_T = 20$ and 40 GeV/c. Characteristics of LTD are estimated in a simple way by applying a variable cut threshold to these distributions. The corresponding (R_g, ε_b) plots for both p_T values are given in Fig.4 .

One can see that at $p_T = 20$ (40) GeV/c the maximum efficiency ε_b^{max} attainable without losing jet separation ability is equal to 0.94 (0.96). At these efficiencies the value of gluon jet rejection factor is $R_g(\varepsilon_b^{max}) = 9(4)$. For LTD discrimiator, R_g appears to be slowly decreasing function of the argument ε_b.

Group B. We have included 2 models of neural nets discriminators into this group.

The first one, labeled "var 0, inp 3", uses three values of summed energy depositions E_1, $(E_2 + E_3)$, E_4 in HC sections. NND(var 0, inp 3) is similar to NND_l discriminator of the "longitudinal" type applied to solving π/μ separation task in [3],[4].

The second model, labeled "var 1, inp 3", differs from NND(var 0,inp 3) in that the third entry E_4 is substituted by $e_{max}^{(4)}$ – the maximum energy deposit among cells in the last HC section.

Characteristics for both NNDs of Group B are presented in Fig.5 for jet $p_T = 20$ and 40 Gev/c

Group C. For all NND models of this group the event features used as inputs are evaluated as functoins of deposited energies in those cells of the first two HC sections that lie inside the 3x3 cell window centered on the position of $e_{max}^{(4)}$ cell in (η, ϕ) plane. The series of NND models are subdivided into 3 subgroups.

Subgroup C1. This subgroup includes one NND model, labeled "var 2, inp 3". The input features for this model are as following.
NND(var 2,inp 3): $E_{c9}^{(1)}$, $E_{c9}^{(2+3)}$, $e_{max}^{(4)}$,   where

$E_{c9}^{(1)}$ – the summed energy deposition in all 9 cells of the 3×3 cell window in HC section 1, and

$E_{c9}^{(2+3)}$ – the corresponding value for the middle section of HC.

In Fig.6 characteristics are presented for the NND of Subgroup C1 at $p_T = 20$ and 40 GeV/c.

Subgroup C2. This subgroup includes 6 NND models:
NND(var k,inp 3), k=3,...,7 and NND(var 8,inp 2).

Along with $e_{max}^{(4)}$, the input features used by models of this subgroup are eveluated as functions of energy depositions in various subsets of cells inside the 3×3 cell window. The subsets of cells and the input features are defined as following.

- NND(var 3,inp 3). Inputs: $E_{c5}^{(1)}$, $E_{c5}^{(2+3)}$, $e_{max}^{(4)}$
  The value E_{c5} is equal to the summed energy deposition in 5 cells whose locations form a cross in the center of the 3×3 cell window.

- NND(var 4,inp 3). Inputs: $E_{c2c}^{(1)}$, $E_{c2c}^{(2+3)}$, $e_{max}^{(4)}$

  E_{c2c} is evaluated as the maximum summed energy deposition among pairs of adjacent cells, one cell of a pair being the central cell of the 3×3 cell window.

- NND(var 5,inp 3). Inputs: $E_{c1c}^{(1)}$, $E_{c1c}^{(2+3)}$, $e_{max}^{(4)}$

  The value of E_{c1c} is equal to energy deposition in the central cell of the 3×3 cell window.

- NND(var 6,inp 3). Inputs: $E_{c2}^{(1)}$, $E_{c2}^{(2+3)}$, $e_{max}^{(4)}$

  The value of E_{c2} is equal to the maximum summed energy deposition among pairs of adjacent cells in the 3×3 cell window.

- NND(var 7,inp 3). Inputs: $E_{c4}^{(1)}$, $E_{c4}^{(2+3)}$, $e_{max}^{(4)}$

  The value of E_{c4} is equal to the maximum summed energy deposition in a 2×2 cell square among four such squares inside the 3x3 cell window.

- NND(var 8,inp 2). Inputs: $E_{c2}^{(2+3)}$, $e_{max}^{(4)}$

  This model does not use information from HC section 1. It may be considered as truncated version of NND(var 6,inp 3) model.

Characteristics for NNDs of Subgroup C2 at $p_T = 20$ and 40 GeV/c are presented in Fig.7.

Subgroup C3. This subgroup includes 6 NND models:
NND(var k,inp 5), k=3,...,7 and NND(var 8,inp 3).
Compared with Subgroup C2, the lengths of input vectors of these models are enlarged by adding information on summed energies E_{c9} in the 3×3 cell windows. The list of input features is as following.

- NND(var 3,inp 5): $E_{c5}^{(1)}$, $E_{c9}^{(1)}$, $E_{c5}^{(2+3)}$, $E_{c9}^{(2+3)}$, $e_{max}^{(4)}$

- NND(var 4,inp 5): $E_{c2c}^{(1)}$, $E_{c9}^{(1)}$, $E_{c2c}^{(2+3)}$, $E_{c9}^{(2+3)}$, $e_{max}^{(4)}$

- NND(var 5,inp 5): $E_{c1c}^{(1)}$, $E_{c9}^{(1)}$, $E_{c1c}^{(2+3)}$, $E_{c9}^{(2+3)}$, $e_{max}^{(4)}$

- NND(var 6,inp 5): $E_{c2}^{(1)}$, $E_{c9}^{(1)}$, $E_{c2}^{(2+3)}$, $E_{c9}^{(2+3)}$, $e_{max}^{(4)}$

- NND(var 7,inp 5): $E_{c4}^{(1)}$, $E_{c9}^{(1)}$, $E_{c4}^{(2+3)}$, $E_{c9}^{(2+3)}$, $e_{max}^{(4)}$

- NND(var 8,inp 3): $E_{c2}^{(2+3)}$, $E_{c9}^{(2+3)}$, $e_{max}^{(4)}$

6

Characteristics for NNDs of Subgroup C3 are presented in Fig.8.

In total there are 13 NND models in Group C. All the models were trained and tested at jet $p_T = 40$ GeV/c. Because of moderate size of event samples available for training NNDs at $p_T = 20$ GeV/c, only models with short input vector (Subgroups C1, C2) were investigated at this p_T value.

Group D. All discriminators of this group are extensions of NND discriminators of the previous Group C. The total number of NND models in Group D is 13.

To get a NND model of the present group, the input vector of the corresponding model from Group C is extended by adding 4 features that are related with distributions in (η, ϕ) plane. The additional inputs are η_m, $\delta\eta_m$, r_m, $R_{1,J}$, where

(η_m, ϕ_m) – parameters of the cell $e_{max}^{(4)}$ with the highest energy deposit in the last depth of HC;

$(\eta_{1,J}, \phi_{1,J})$ – parameters of the jet axis estimated with the use of active cells in the first HC section,

$\delta\eta_m = (\eta_m - \eta_{1,J})$, $\delta\phi_m = (\phi_m - \phi_{1,J})$, $r_m = \sqrt{\delta\eta_m^2 + \delta\phi_m^2}$ -are deviations of the cell $e_{max}^{(4)}$ from the jet axis in (η, ϕ) plane,

$R_{1,J}$ – estimation of the jet radius in (η, ϕ) plane with the use of energy depositions in cells of the first HC section.

In estimating values of $\eta_{1,J}$, $\phi_{1,J}$, $R_{1,J}$ we follwed the procedures proposed in [6], [7] for reconstruction of jet parameters using calorimetric data:

$$\eta_{1,J} = \frac{1}{E_{T,J}} \times \sum_i e_{T,i}\eta_i$$

$$\phi_{1,J} = \frac{1}{E_{T,J}} \times \sum_i e_{T,i}\phi_i$$

$$E_{T,J} = \sum_i e_{T,i}$$

$$R_{1,J} = \frac{1}{E_{T,J}} \times \sum_i r_i e_{T,i} ,$$

where $e_{T,i}$ – transverse energy deposited in i-th cell of HC section 1.

In Fig.9 distributions of η_m, $\delta\eta_m$, r_m and $R_{1,J}$ at $p_T = 40$ GeV/c are presented for subsets of gluon and b-jets in which the condition $0.4 < e_{max}^{(4)} < 1.2$ GeV is satisfied.

In Fig.10 characteristics are presented for those discriminators of Group D at $p_T = 40$ GeV/c which are extensions of NN discriminators from Subgroup

7

C3. It should be noted that the values of R_g attained by NNDs of Group D exceed R_g values of Subgroup C3 only at lower efficiencies $\varepsilon_b < 0.8$.

Group E. All discriminators of this group are extensions of NND discriminators of Group D. The corresponding input vectors used in Group D are extended by adding 2 features: E_1 and $(E_2 + E_3)$, where E_k is the summed energy deposition in k-th HC section. The input vectors of discriminators in Group E contain values of 11 features.

Though formally the Group E may include many NND models, we have tested only one NND model with full length input vector at $p_T = 40$ GeV/c, namely NND (var 6, inp 11). Its characteristics are presented in Fig.11.

Subgroup E1. This subgroup is a truncated version of NNDs from Group E. The following features are used as inputs to the perceptron (6, 4, 1) trained at $p_T = 20$ GeV/c : E_{c2}, $e_{max}^{(4)}$, η_m, $\delta\eta_m$, r_m, $R_{1,J}$. Characteristics of NND(var 6, inp 6) are presented in Fig.12.

Neural nets were trained using up to 10^4 epochs in a training session. As an example we present in Fig.13 the dynamics of mean fit errors MFE as functions of the current epoch number in training sessions for several NNDs.

Using (R_g, ε_b) plots a reader can compare performances of LTD and various NND models in a straightforward way. Though the idea of another jet classifier was formulated in [2], the corresponding plots on its performance were not given. Nevertheless, using charcteristics of our wide set of neural net discriminators we can estimate upper bounds for performance of the classifier [2]. The feasibility lies in the fact that a classifier which performs classification by applying n consecuitive cuts to one-dimentional distributions of event features, in general case, is inferior to a classifier which uses m hyperplanes $(m \geq n)$ for separation of event classes directly in n-dimensional features space. Among the wide set of NNDs, the NND(var 8, inp 2) is the most close one to the classifier [2]. Though input variables are the same ($E_{c2}^{(2+3)}$ and $e_{max}^{(4)}$), the number of free parpmeters in NND case is bigger (4 hyperplanes are used at $p_T = 20$ GeV/c, 6 hyperplanes at $p_T = 40$ GeV/c).

For convenience we summarize the results in Table 1, 2 , where gluon jets rejection factors are given at $p_T = 20$ and 40 GeV/c for 3 values of b-jet identification efficiencies ($\varepsilon_b = 0.90$, 0.85, 0.80) for   a) the best of NND, b) LTD and   c) NND(var 8, inp 2).

5   Conclusion

1. The use of linear threshold discriminator (LTD) that performs classification of jets by applying a cut on summed energy deposition in the last

depth of Tile Calorimeter leads to poor performance: at b-jet identification efficiencies $0.80 < \varepsilon_b < 0.95$ the gluon jet rejection factor R_g lies in the range 13 - 17 (for $p_T = 20$ GeV/c) and in the range 6 - 8 (for $p_T = 40$ GeV/c).

2. Results on more than 20 models of neural net discriminators (NND) show appreciably higher performance of NND compared to LTD. At b-jet identification efficiencies $0.80 < \varepsilon_b < 0.90$ the gluon jet rejection factor R_g is 4 - 6 times higher for NND at $p_T = 20$ GeV/c and 5 - 10 times higher at $p_T = 40$ GeV/c.

3. To reveal the full potential of ANN approach to solving jet separation tasks, greater samples of events are needed to allow using neural nets of a size bigger than in the present investigation.

4. Accepting the present results as an estimate of lower bounds of NND performances, one can state that the following inequalities should hold for the gluon jet rejection factor $R_g(\varepsilon_b)$ attained by NND:

   (a) at $p_T = 20$ GeV/c : $R_g(0.90) \geq 50$, $R_g(0.85) \geq 100$
   (b) at $p_T = 40$ GeV/c : $R_g(0.90) \geq 30$, $R_g(0.85) \geq 70$

Table 1:   Gluon jet rejection factors at $p_T = 20$ GeV/c

ε_b	Best of NND	LTD	NND (var 8, inp 2)
0.80	100	17	70
0.85	100	15	70
0.90	50	13	. 30

Table 2:   Gluon jet rejection factors at $p_T = 40$ GeV/c

ε_b	Best of NND	LTD	NND (var 8, inp 2)
0.80	80	8	20
0.85	70	7	. 15
0.90	30	6	10
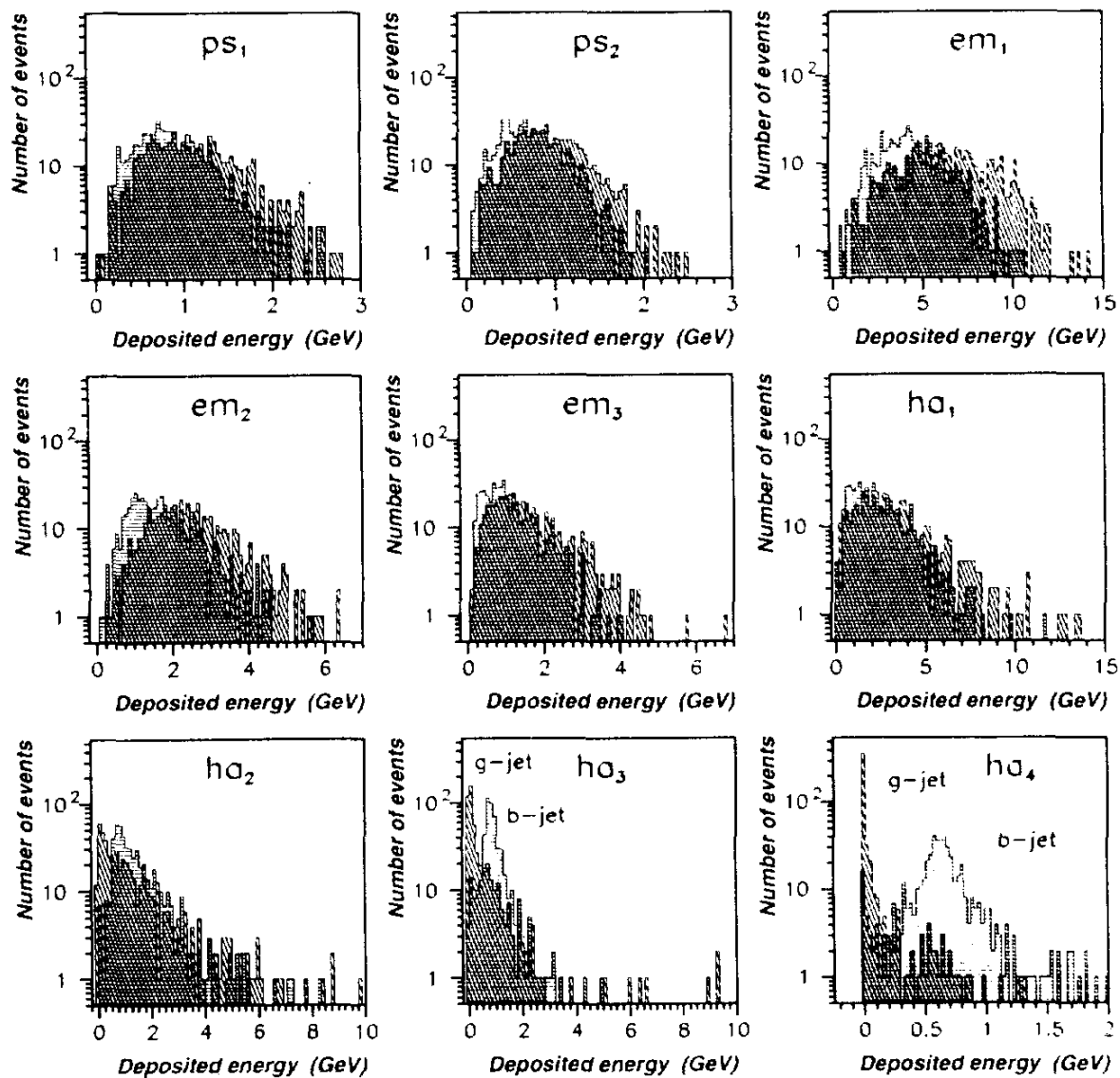
Figure 1: *Distributions of deposited energies in sections of preshower detector (ps₁, ps₂), EM calorimeter (em₁ − em₃), Hadron calorimeter (ha₁ − ha₄) for b-jets and gluon jets at p_T = 20 GeV/c in the central region $0 < \eta < 0.6$*
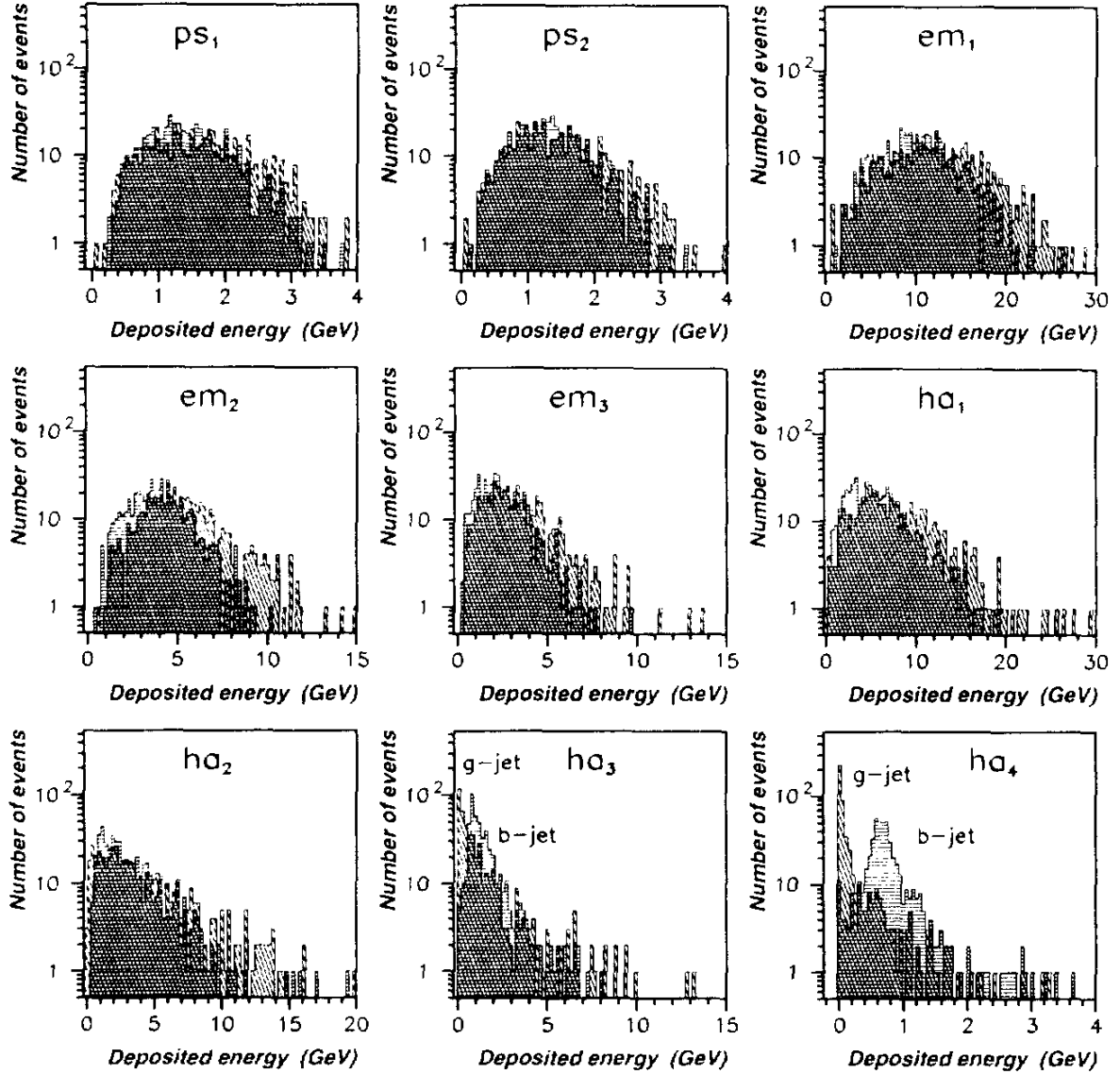
Figure 2: *Distributions of deposited energies in sections of preshower detector* (*ps*₁, *ps*₂), *EM calorimeter* (*em*₁ − *em*₃), *Hadron calorimeter* (*ha*₁ − *ha*₄) *for b-jets and gluon jets at* $p_T = 40$ *GeV/c in the central region* $0 < \eta < 0.6$

E4 distribution
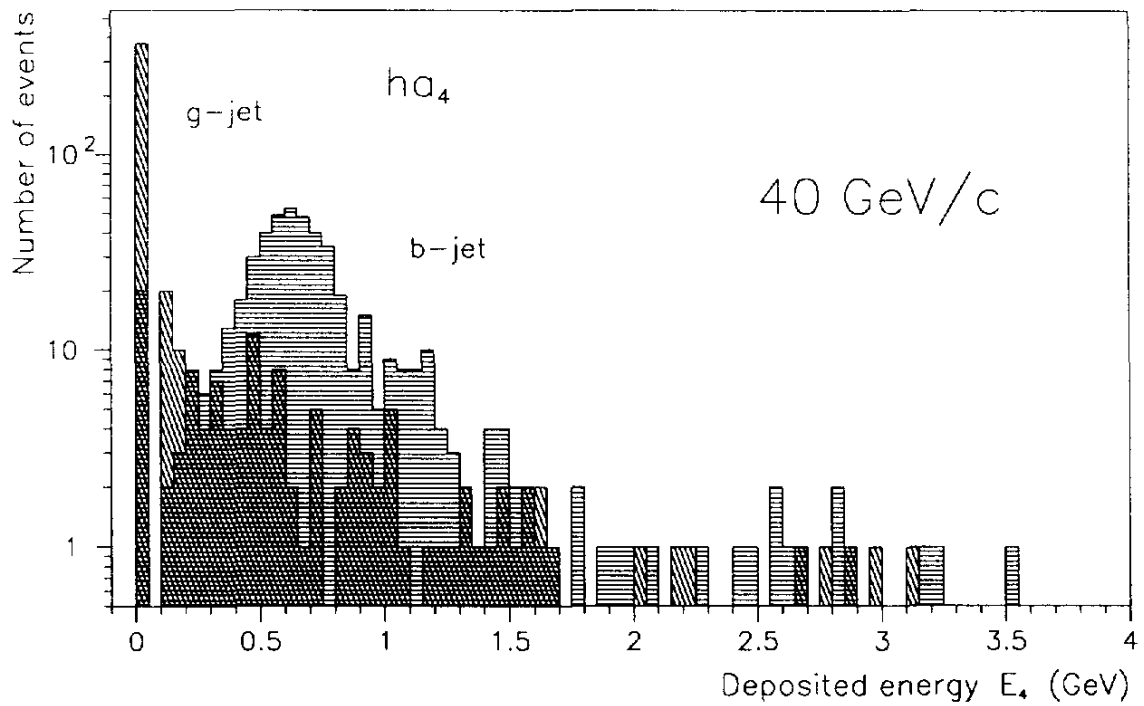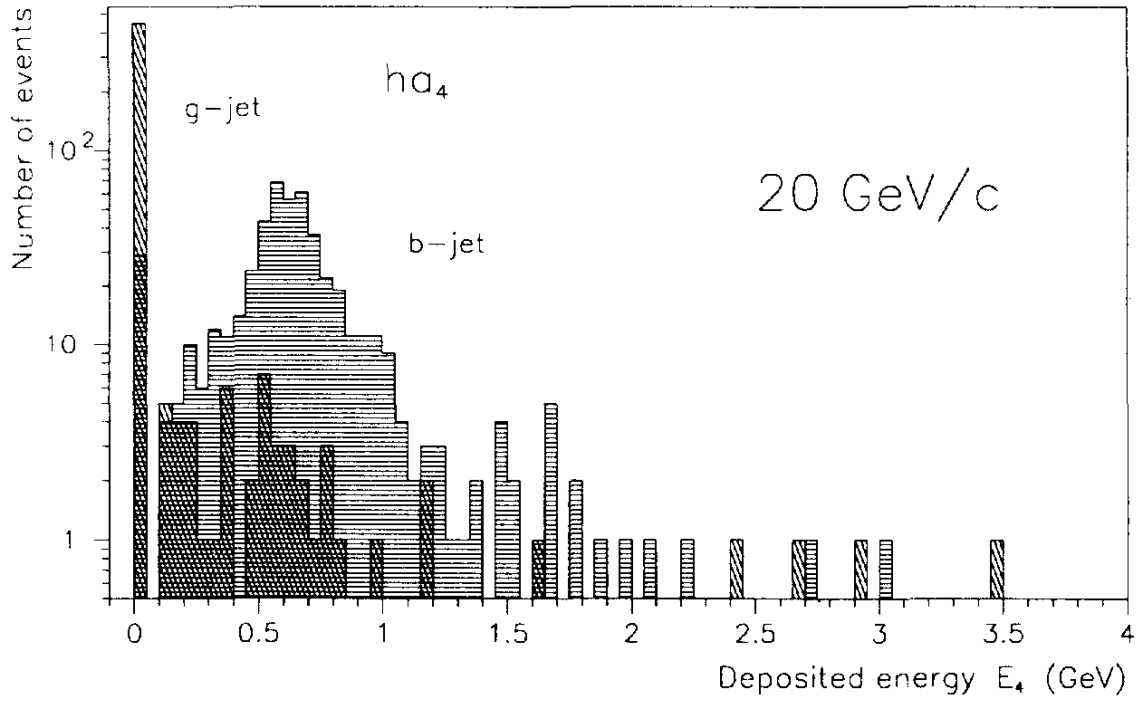
Figure 3: *Distribution of summed energy deposition E_4 in the last HC section for jets at $p_T = 20$ and 40 GeV/c*

Jets separation by LTD
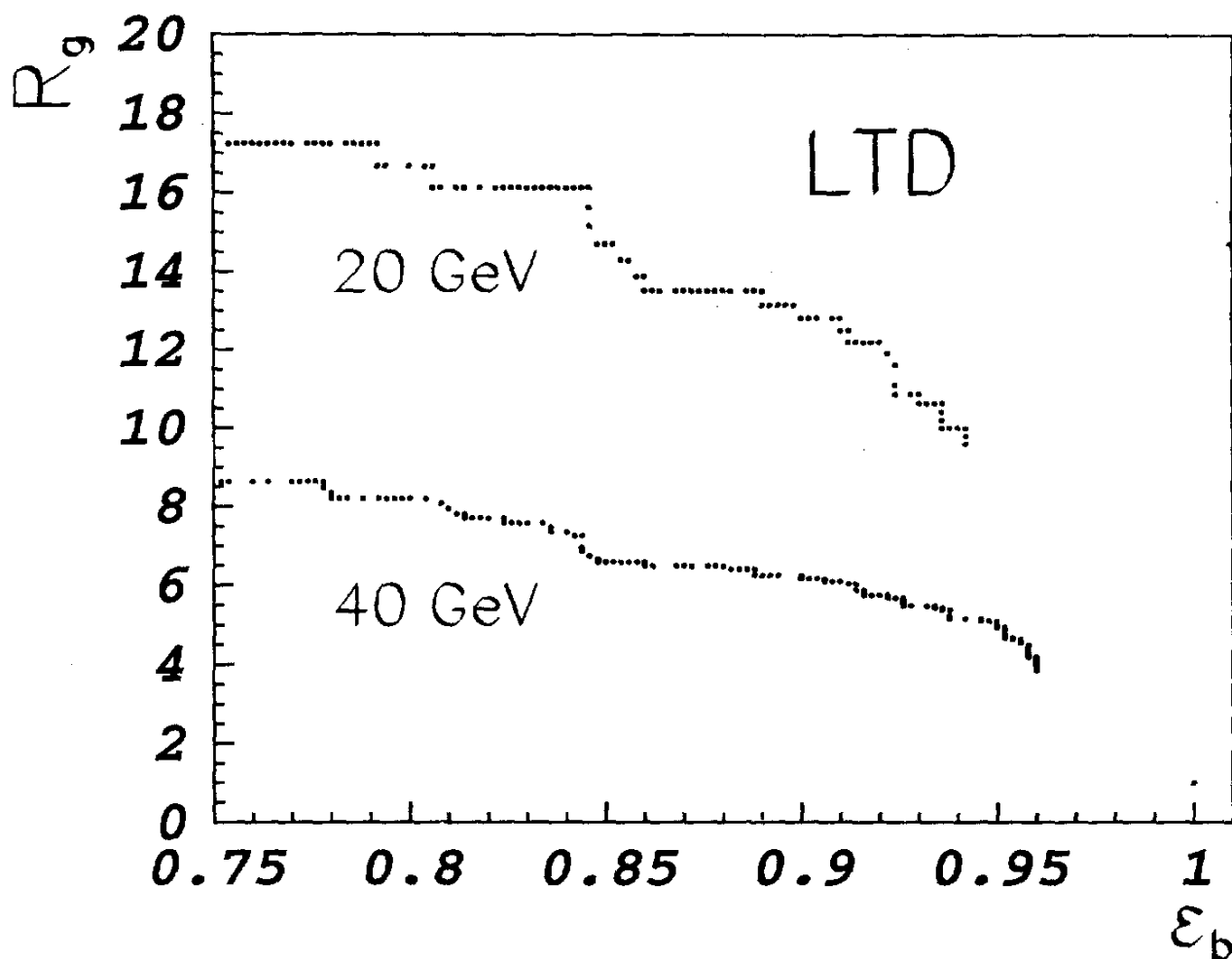
Figure 4: *Linear threshold discriminator* **LTD**: *gluon jet rejection factor R_g versus b-jets identification efficiency ε_b at p_T = 20 and 40 GeV/c*
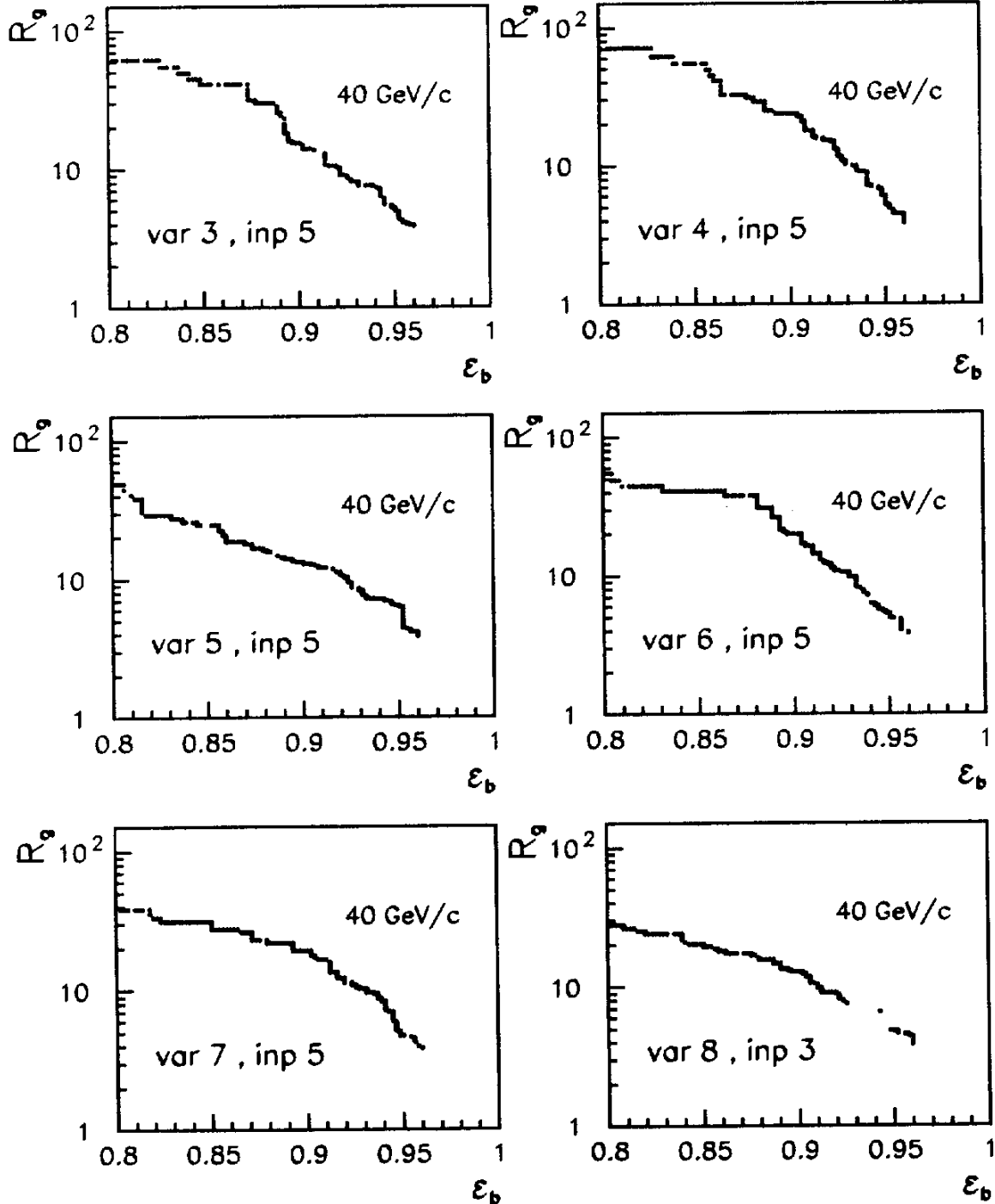
Jets separation by NND
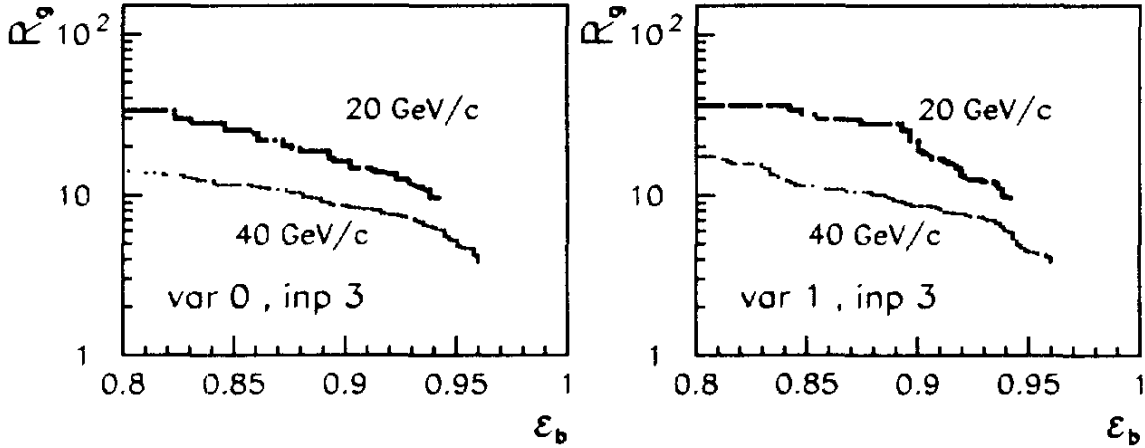
Figure 5: **Group B:** *Gluon jets rejection factor R_g versus b-jets identification efficiency ε_b at p_T = 20 and 40 GeV/c*

Jets separation by NND
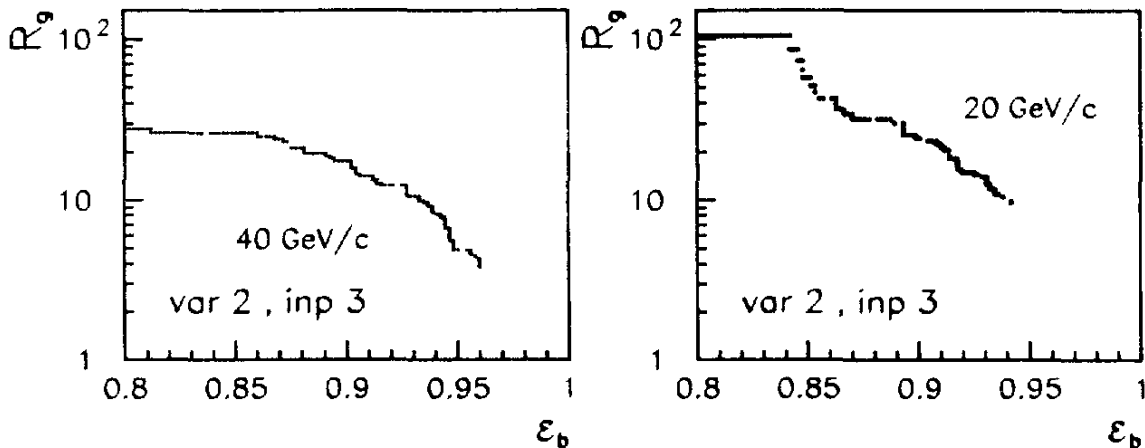
Figure 6: **Subgroup C1:** *Gluon jets rejection factor R_g versus b-jets identification efficiency ε_b at p_T = 20 and 40 GeV/c*

Jets separation by NND
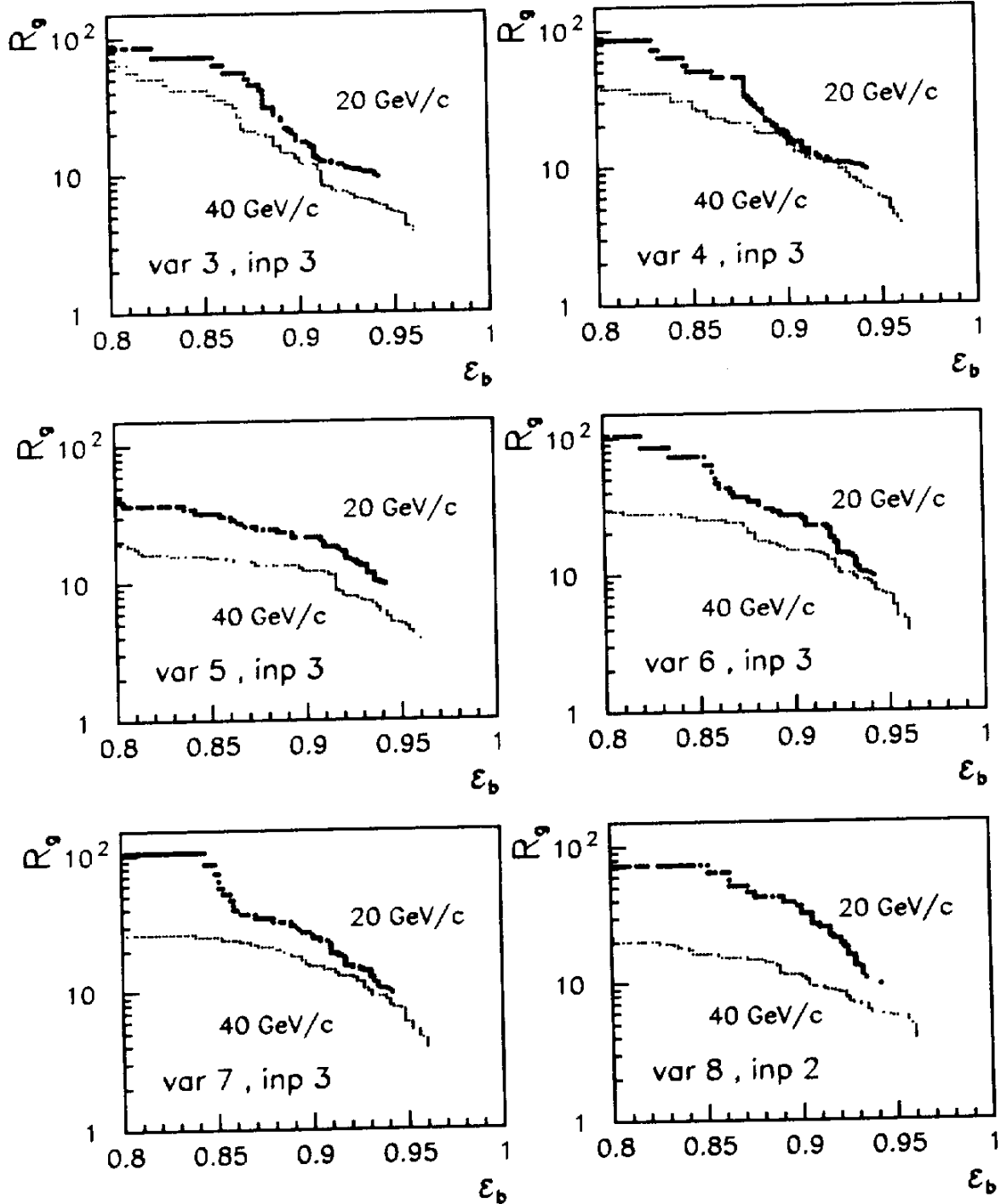
Figure 7: **Subgroup C2:** *Gluon jets rejection factor R_g versus b-jets identification efficiency ε_b at $p_T = 20$ and 40 GeV/c*

Jets separation by NND

Figure 8: **Subgroup C3:** *Gluon jets rejection factor R_g versus b-jets identification efficiency ε_b at $p_T = 40$ GeV/c*

Angular features at 40 GeV/c
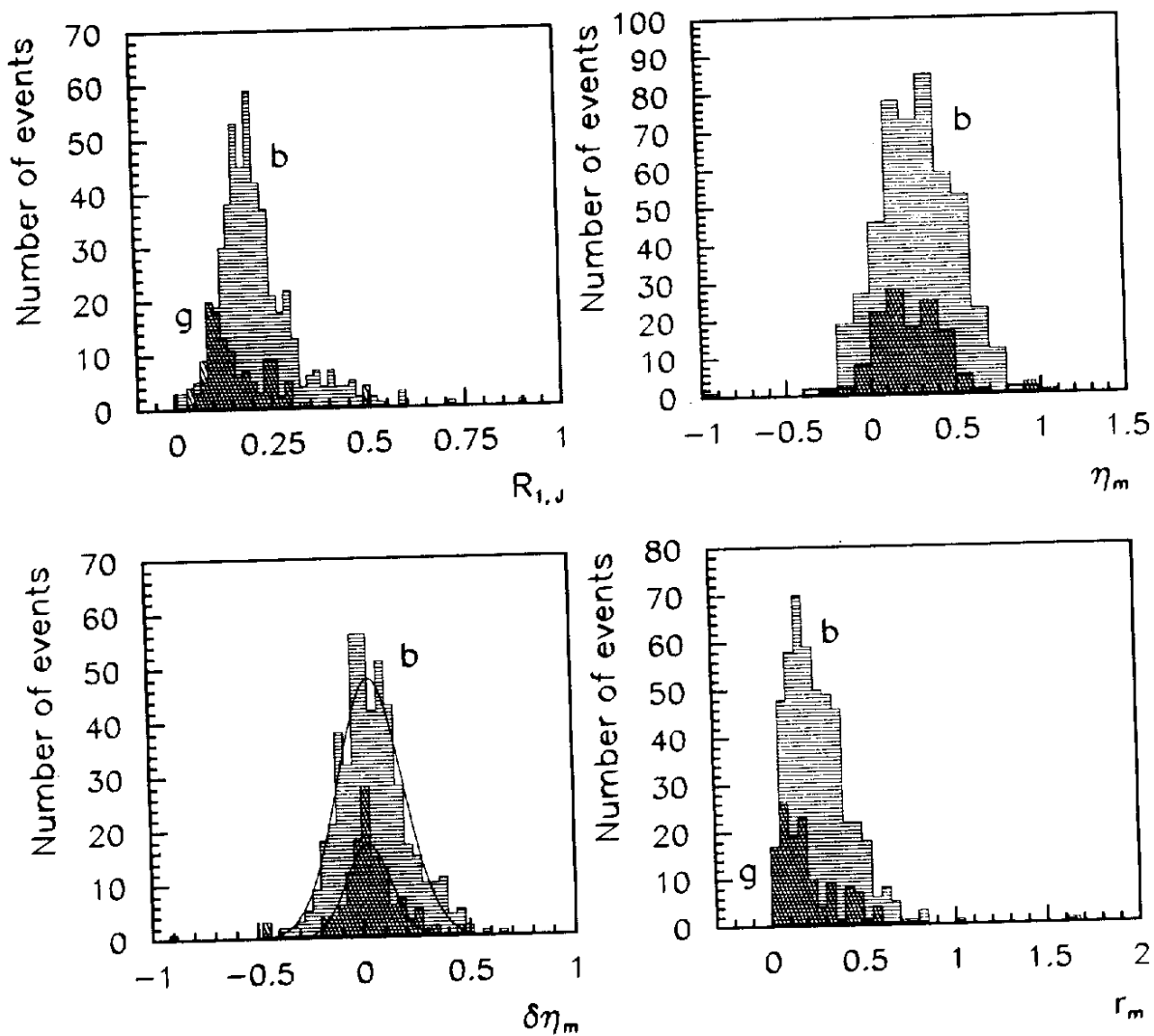
Figure 9: *Distributions of angular features* η_m, $\delta\eta_m$, r_m *and* $R_{1,J}$ *at* $p_T = 40$ *GeV/c for subsets of jets with* $0.4 < e_{max}^{(4)} < 1.2$ *GeV/c*

18

Jets separation by NND
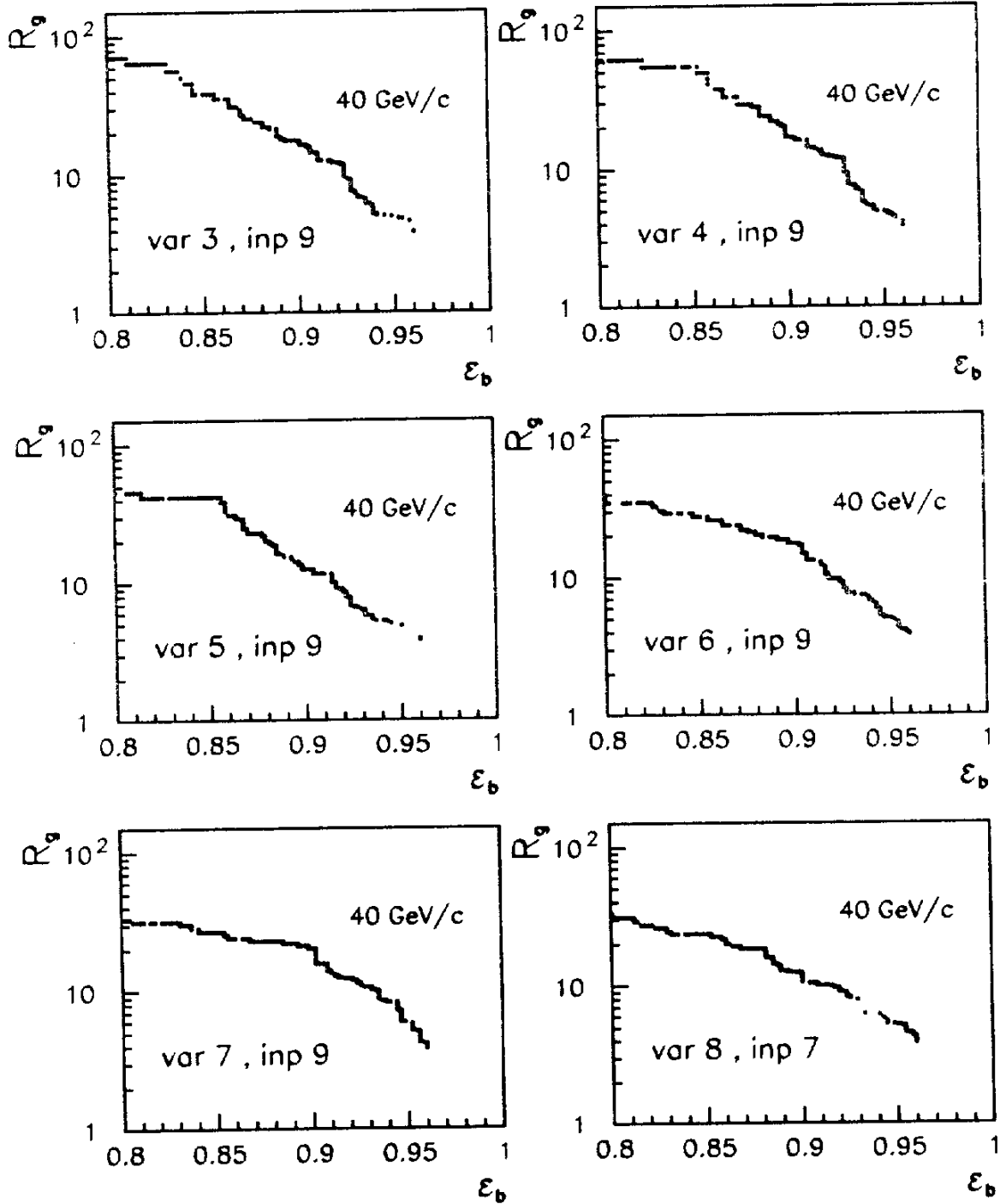
Figure 10: **Group D:** *Gluon jets rejection factor* R_g *versus b-jets identification efficiency* ε_b *at* $p_T = 40\ GeV/c$

Jets separation by NND

Jets separation by NND
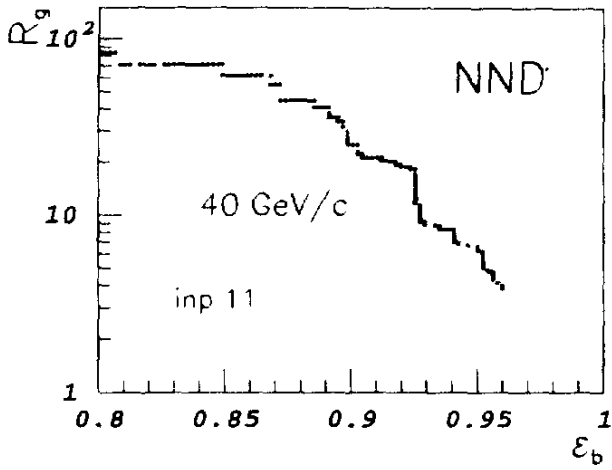
Figure 11: **Group E:** *Gluon jets rejection factor R_g versus b-jets identification efficiency ε_b at $p_T = 40$ GeV/c*
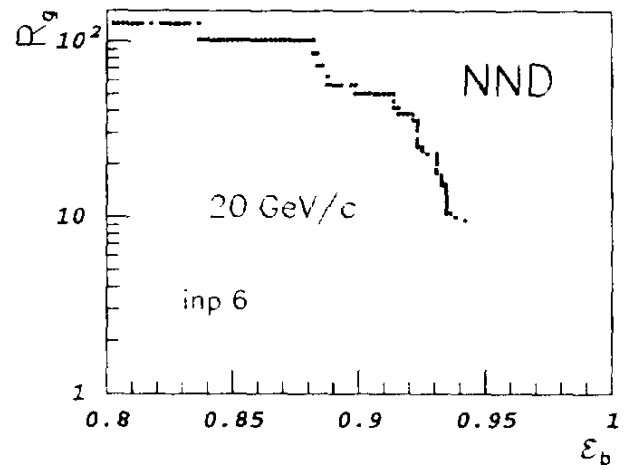
Figure 12: **Subgroup E1:** *Gluon jets rejection factor R_g versus b-jets identification efficiency ε_b at $p_T = 20$ GeV/c*

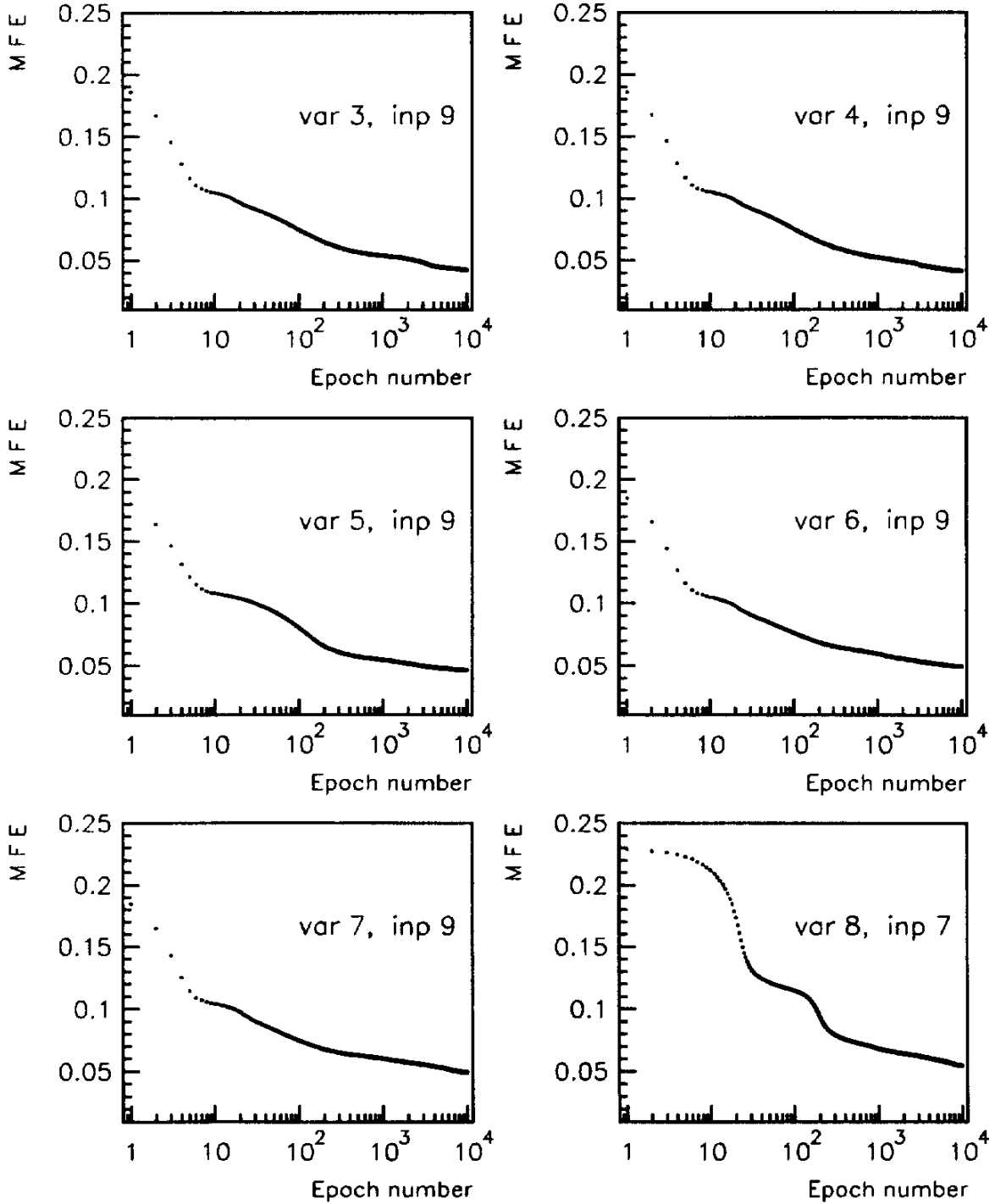# Mean fit errors in training sesions (40 GeV/c)

Figure 13: *Dynamics of mean fit error MFE in training sessions for NNDs of Group D at p_T = 40 GeV/c*

References

[1] J.Budagov, I.Chirikov-Zorin, A.Pantea, D.Pantea, O.Pukhov, M.Bosman, M.Nessi, "B-meson tagging improvement using HCAL information", ATLAS Internal Note, TILECAL-NO-023 (1994)

[2] J.Budagov, D.Pantea, M.Bosman, M.Nessi "Low p_T Muons in B-jets in ATLAS Tilecal", ATLAS Int.Note TILECAL-NO-062 (1995)

[3] A.Astvatsaturov, J.Budagov, I.Chirikov-Zorin, D.Pantea, A.Paplevka, V.Shigaev, S.Sushkov, M.Bosman, M.Nessi "Impovement in π/μ separation at low p_T in ATLAS Hadron Calorimeter using artificial neural networks technique", ATLAS Int.Note, TILECAL-NO-060 (1995)

[4] A.Astvatsaturov, J.Budagov, I.Chirikov-Zorin, D.Pantea, A.Paplevka, V.Shigaev, S.Sushkov, M.Bosman, M.Nessi "Impovement in π/μ separation of isolated muon and pions at low p_T in ATLAS Hadron Calorimeter using artificial neural networks technique", Commun. of JINR, E10-95-476, Dubna, 1995

[5] ATLAS, "Technical Proposal for a General-Purpose pp Experiment at the Large Hadron Collider at CERN", CERN/LHCC/94-43, LHCC/P2 (1994)

[6] F.Abe at al. "Measurement of Jet Shapes in $p\bar{p}$ Collisions at $\sqrt{s} = 1.8$ TeV", Phys. Rev. Lett. 70, 713 (1993)

[7] S.D.Ellis, Z.Kunszt and D.E.Soper", One-Jet Inclusive Cross Section at Order α_s^3: Quarks and Gluons", Phys. Rev. Lett 64, 2121 (1990)

[8] C.Peterson, T.Rögnvaldsson and L.Lönnblad, "JETNET 3.0 - A versatile Artificial Neural Network Package", Comp. Phys. Commun. **81** (1994) 185

The Publishing Department
of the Joint Institute for Nuclear Research
offers you to acquire the following books:

Index	Title
E7-93-274	Proceedings of the International School-Seminar on Heavy Ion Physics. Dubna, 1993 (2 volumes, 498 and 590 pp., stiffened cover, in English)
Д14-93-325	Proceedings of the Workshop «Activation Analysis in Environment Protection». Dubna, 1992 (in Russian and English)
Д1,9,13-93-459	Proceedings of the II Workshop on JINR Tau-Charm Factory. Dubna, 1993 (266 p. in Russian and English)
E7-94-19	Proceedings of the International Conference on Dynamical Aspects of Nuclear Fission. Smolenice, 1993 (318 p. in English)
94-55	Proceedings of the International Bogoliubov Memorial Meeting. Dubna, 1993 (216 p. in Russian and English)
E2-94-95	Proceedings of the International Symposium «Dubna Deuteron-93». Dubna, 1993 (390 p. in English)
Д14-94-269	Abstracts of the XXX Conference on Low Temperature Physics. Dubna, 1994 (2 volumes in Russian and English)
E7-94-270	Proceedings of the Workshop on Physical Experiments and First Results on Heavy Ion Storage and Cooler Rings. Smolenice, 1992 (324 p. in English)
E13-94-290	Abstracts of the 17th International Conference «Nuclear Tracks in Solids». Dubna, 1994 (296 p. in English)
E2-94-347	International Workshop «Symmetry Methods in Physics». In Memory of Professor Ya.A.Smorodinsky. Dubna, 1993 (2 volumes, 602 p. in English)
E4-94-370	Proceedings of the IV International Conference on Selected Topics in Nuclear Structure. Dubna, 1994 (412 p. in English)
E4-94-386	Proceedings of the VI Trilateral German-Russian-Ukrainian Seminar on High-Temperature Superconductivity. Dubna, 1994 (340 p. in English)
D2-94-390	D.I.Blokhintsev. Proceedings of the Seminars. Dedicated to the 85th Anniversary of the Birthday of D.I.Blokhintsev. Dubna, 1995 (271 p. in Russian and English)

Index	Title
E3-94-419	Proceedings of the II International Seminar on Neutron-Nucleus Interactions (ISINN-2) «Neutron Spectroscopy, Nuclear Structure, Related Topics». Dubna, 1994 (363 p. in English)
D13-94-491	Proceedings of the XVI International Symposium on Nuclear Electronics and VI International School on Automation and Computing in Nuclear Physics and Astrophysics. Varna, 1994 (246 p. in Russian and English)
D13,14-95-49	Proceedings of the International Symposium on Muon and Pion Interactions with Matter. Dubna, 1994 (304 p. in Russian and English)
D3-95-169	Proceedings of the International Seminar ADVANCED PULSED NEUTRON SOURCES: Physics of/at ADVANCED Pulsed Neutron Sources. PANS-II. Dubna, 1994 (336 p. in Russian and English)
D1-95-305	Proceedings of the XVII Workshop on Neutrino Detector IHEP—JINR. Dubna, 1995 (178 p. in Russian and English)
E3-95-307	Proceedings of the III International Seminar on Interaction of Neutrons with Nuclei. Neutron Spectroscopy, Nuclear Structure, Related Topics. Dubna, 1995 (356 p. in English)
D4-95-308	V.G.Soloviev. Frontiers in Nuclear Physics. Dedicated to the 70th Anniversary of the Birthday of V.G.Soloviev. Dubna, 1995 (238 p. in Russian and English)
D3,14-95-323	VII School on Neutron Physics. Lectures. Vol.1. Dubna, 1995 (356 p. in Russian and English)
E10,11-95-387	Proceedings of the ESONE International Conference RTD'94 on REAL TIME DATA 1994 with Emphasis on Distributed Front-End Processing. Dubna, 1994 (358 p. in English)

Please apply to the Publishing Department of the Joint Institute for Nuclear Research for extra information. Our address is:

Publishing Department
Joint Institute for Nuclear Research
Dubna, Moscow Region
141980 Russia
E-mail: publish@pds.jinr.dubna.su.

С использованием системного подхода исследуется возможность повышения эффективности идентификации мюонов с малым значением поперечного импульса p_T (2 < p_T < 5 ГэВ/с) в составе b-струй, регистрируемых адронным калориметром ATLAS. В центральной области калориметра 0 < η < 0,6 для p_T = 20 и 40 ГэВ/с были применены более двадцати моделей нейросетевых дискриминаторов (NND) для разделения глюонных струй и b-струй (с одним «мягким» мюоном в составе b-струй). Характеристики дискриминаторов NND сравниваются с характеристиками порогового дискриминатора (LTD), осуществляющего классификацию струй посредством порогового сравнения величины суммарного энерговыделения в последней секции адронного калориметра. Показано, что в сравнении с LTD при эффективности регистрации b-струй 0,80 < ε_b < 0,90 фактор режекции глюонных струй R_g в случае дискриминаторов NND повышается в 4-10 раз.

Полученные результаты основаны на анализе данных 2000 струй, полученных при помощи программ моделирования ATLAS.

Работа выполнена в Лаборатории ядерных проблем ОИЯИ.

The possibility to enchance the capability of ATLAS Tile Calorimeter to identify low p_T muons (2 < p_T < 5 GeV/c) inside b-jets by the use of artificial neural networks technique is investigated in a systematic way. More than 20 models of neural net discriminators (NND) were applied to separation of gluon jets and b-jets (with a single soft muon inside a b-jet) at jet p_T = 20 and 40 GeV/c in the central region 0 < η < 0.6. Characteristics of NND are compared to those of the linear threshold discriminator (LTD) which performs jet classification by applying a cut to the summed energy deposition in the last depth of Tile Calorimeter. It is shown that at b-jet identification efficiencies 0.80 < ε_b < 0.90 the gluon jet rejection factor R_g is 4-10 times higher in NND case compared to LTD.

The results obtained are based on 2000 jets simulated with the use of ATLAS simulation programs.

The investigation has been performed at the Laboratory of Nuclear Problems, JINR.

Макет Т.Е.Попеко